Chemico-Biological Interactions 309 (2019) 108699

Contents lists available at ScienceDirect

Chemico-Biological Interactions

journal homepage: www.elsevier.com/locate/chembioint

The four-helix bundle in cholinesterase dimers: Structural and energetic determinants of stability

Dana A. Novichkova[a], Sofya V. Lushchekina[a,*], Orly Dym[b], Patrick Masson[c], Israel Silman[b], Joel L. Sussman[b]

[a] N.M. Emanuel Institute of Biochemical Physics of Russian Academy of Sciences, 4 Kosygina St., Moscow, 119334, Russia
[b] Weizmann Institute of Science, 234 Herzl St., Rehovot, 7610001, Israel
[c] Kazan Federal University, Neuropharmacology Laboratory, 18 Kremlevskaya St., Kazan, 420008, Russia

ARTICLE INFO

Keywords:
Acetylcholinesterase
Butyrylcholinesterase
Dimerization
Four-helix bundle
&Mcy
Markov state model
Free energy perturbation
In silico alanine screening
Replica exchange

ABSTRACT

The crystal structures of truncated forms of cholinesterases provide good models for assessing the role of non-covalent interactions in dimer assembly in the absence of cross-linking disulfide bonds. These structures identify the four-helix bundle that serves as the interface for formation of acetylcholinesterase and butyrylcholinesterase dimers. Here we performed a theoretical comparison of the structural and energetic factors governing dimerization. This included identification of inter-subunit and intra-subunit hydrogen bonds and hydrophobic interactions, evaluation of solvent-accessible surfaces, and estimation of electrostatic contributions to dimerization. To reveal the contribution to dimerization of individual amino acids within the contact area, free energy perturbation alanine screening was performed. Markov state modelling shows that the loop between the α13 and α14 helices in BChE is unstable, and occupies 4 macro-states. The order of magnitude of mean first passage times between these macrostates is $\sim 10^{-8}$ s. Replica exchange molecular dynamics umbrella sampling calculations revealed that the free energy of human BChE dimerization is −15.5 kcal/mol, while that for human AChE is −26.4 kcal/mol. Thus, the C-terminally truncated human butyrylcholinesterase dimer is substantially less stable than that of human acetylcholinesterase. An animated Interactive 3D Complement (I3DC) is available in Proteopedia at http://proteopedia.org/w/Journal:CHEMBIOINT:1.

1. Introduction

Investigation of protein oligomerization and characterization of the interactions between protein subunits is of great importance because physiologically active forms of many proteins are oligomers. Both cholinesterases (ChEs) - acetylcholinesterase (AChE) and butyrylcholinesterase (BChE) - naturally occur as repertoires of molecular forms that contain different numbers of catalytic subunits, *viz.*, monomers, dimers, tetramers, and larger collagen-tailed species [1]. Quaternary assembly of anchored and soluble forms of ChEs has been investigated for over 50 years [2,3]. In an applied context, stabilization of recombinant forms in the bloodstream is of pharmacokinetic significances [4]. *In vivo*, disulfide bonds are formed between individual monomers and/or between the monomers and the anchoring polypeptides [5–7], ColQ and PRiMA [8]. Various truncated forms of ChE, obtained from *Tc*AChE [9], mAChE [10], hAChE [11], *Dm*AChE [12] and hBChE [13], are devoid of the amino acid sequence at their C-termini that contains the Cys residue involved in formation of disulfide-bonded dimers. Such truncated forms have been used to obtain crystal structures in which the monomers are bound to each other only *via* non-covalent interactions. In particular, partial interconversion between monomeric and dimeric forms of hBChE was observed by non-denaturing gel electrophoresis [14].

All crystal structures of AChE deposited in the PDB (https://www.rcsb.org [15]) display dimers in which the monomers associate through an antiparallel four-helix bundle. With respect to BChE, crystal structures have been obtained only for monomeric forms of hBChE. In the first hBChE crystal structure obtained (PDB ID 1P0I [16]), of partially glycosylated enzyme expressed in CHO cells, dimers assembling *via* a four-helix bundle were not observed (Fig. 1B) [17]. Subsequently,

Abbreviations: AChE, acetylcholinesterase; BChE, butyrylcholinesterase; ChEs, cholinesterases; COM, center of mass; FEP, free energy perturbation; MD, molecular dynamics; MSM, Markov state model; PMF, potential of mean force; SASA, solvent available surface area; TICA, time-lagged independent component analysis; REMD-US, replica exchange molecular dynamics umbrella sampling

* Corresponding author.
E-mail address: sofya.lushchekina@gmail.com (S.V. Lushchekina).

https://doi.org/10.1016/j.cbi.2019.06.012
Received 15 March 2019; Received in revised form 30 May 2019; Accepted 6 June 2019
Available online 13 June 2019
0009-2797/

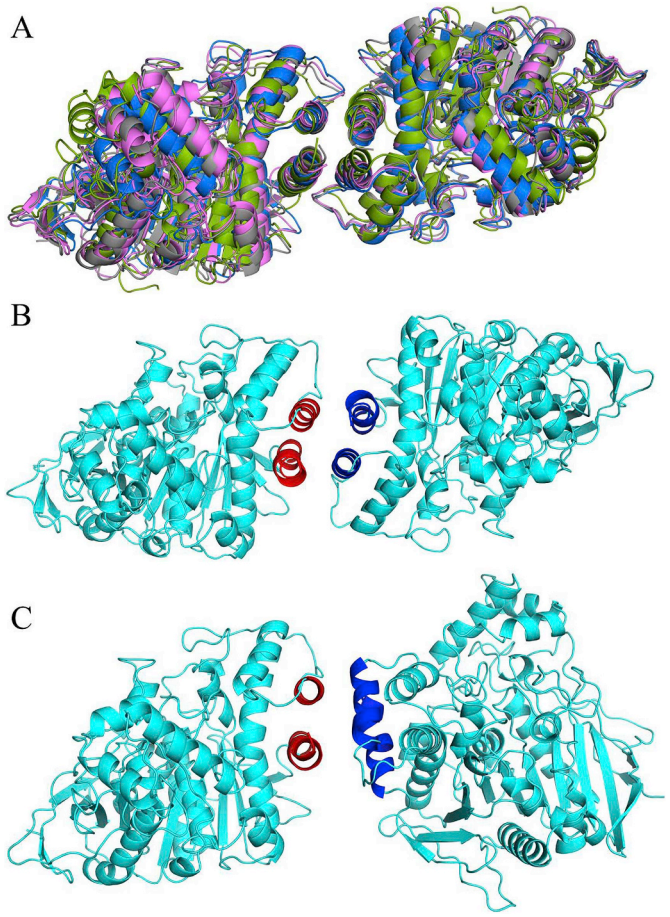

Fig. 1. (A) Aligned crystal structures of AChEs from different species: pink, hAChE (PDB ID 4EY4); gray, mAChE (PDB ID 1J06); blue, *Tc*AChE (PDB ID 1W76); green, *Dm*AChE (PDB ID 1QO9). (B) Crystal structure of hBChE displaying a dimer assembled *via* an antiparallel four-helix bundle (PDB ID 4AQD); (C) Crystal structure of hBChE devoid of a four-helix bundle (PDB ID 1P0I).

however, a crystal structure in which the dimers did assemble *via* a four-helix bundle (PDB ID 4AQD) was obtained for fully glycosylated hBChE expressed in *Drosophila* S2 cells (Fig. 1A) [18]. This dissimilarity of the two crystal structures reveals the high sensitivity of hBChE dimerization to the expression system and crystallization conditions.

The four-helix bundle motif occurs in oligomers of many proteins. In the ChEs, the dimer is a well-packed structure arranged in an up-down topology, with the bundle involving two helices, α13 and α18-19, from each monomer.

Organization of ChEs' tryptophan amphiphilic tetramerization domains around core proline-rich peptides is described by X-ray crystallography for AChE [19], and by cryo-EM structures of BChE tetramers in recent publications [20,21]. In the following, we describe a comparative analysis of hAChE and hBChE dimers assembly, considering only the truncated forms devoid of the tetramerization domains. To identify the most important amino acids involved in interactions between subunits *via* the four-helix bundles free energy perturbation (FEP) computational alanine screening was performed [22,23]. Molecular dynamics (MD) simulations with Markov chain analysis were used to describe the dynamics of subunits in solution, and to locate metastable conformations of sequence segments involved in dimerization. Potential of mean force (PMF) calculations [24,25] were used to estimate the free energy of dimerization for both hAChE and hBChE.

2. Methods

2.1. Sequence alignment

To compare the primary structure of cholinesterases, sequences were aligned using UniProt Align [26].

2.2. Preliminary structure preparation

Among crystallographic structures of cholinesterases available in the PDB database, we selected several structures with high resolution and a low number of missing residues: hAChE (PDB ID 4EY4 [27]), mAChE (PDB ID 1J06 [28]), *Tc*AChE (PDB ID 1W76 [29]), hBChE (PDB ID 4AQD [18]). The missing residues were added by means of the Modeller 9.14 program [30], and histidine protonation states were estimated using Reduce [31]. For MD simulations, systems were prepared with tools of the VMD program [32]. Proteins were solvated with TIP3P water molecules to produce rectangular solvent shells with boundaries not less than 10 Å from the protein. Na^+ and Cl^- were added to electroneutralize the systems at a final concentration of 0.15 M.

2.3. Molecular dynamics simulations

MD simulations utilized NAMD 2.12 [33] with the CHARMM36 force field [34], under a pressure of 1 bar and temperature off 298 K, with the Langevin thermostat and barostat, and 1 fs time steps, on the Lomonosov-2 supercomputer [35]. The prepared structures were first minimized during 2000 steps with coordinates of the heavy atoms of the proteins fixed as in the crystal structures, and the solvation shells were then equilibrated during 500 ps with all protein coordinates remaining fixed. Structures prepared in this manner were used for all subsequent constrained and unconstrained simulations. For each system, 3 parallel unconstrained runs of 100 ns were performed, and the trajectories were used for analysis of interactions in the dimers. Constrained simulations are described below.

2.4. Hydrophobic interactions

To estimate apolar interactions, the number of hydrophobic contacts between monomers was counted. Hydrophobic elements were amino acids whose side chains lacked charged and hydroxyl groups (*i.e.* Ala, Val, Ile, Leu, Cys, Met, Phe and Trp). Hydrophobic contacts were considered for pairs of side chains of these residues within a distance of 5 Å.

A second approach was also used to estimate apolar interactions *via* the measurement of the reduction in solvent-accessible surface area (SASA) of subunits upon dimerization, excluding charged amino acids (Asp, Glu, Lys, Arg), using a 1.4 Å probe radius [36].

2.5. Electrostatic energy of dimerization

Electrostatic energy of dimerization was calculated with the Adaptive Poisson-Boltzmann Solver (APBS) program [37] as described in [38].

The Coulomb energy of binding was calculated on the *i*-th atom as a product of potential induced from another monomer to the place in space of the *i*-th atom and charge of the *i*-th atom (atomic charges from force fields PARSE [39], CHARMM [34], AMBER [40] assigned by the PDB2PQR program [41]):

$$E_{Coul} = \sum_{i=1}^{n} \phi_i q_i \quad (1)$$

Where ϕ_i is the potential, and q_i is the charge of each ion.

The electrostatic dimerization energy is the sum of the desolvation energy and the Coulomb energy of binding [42]:

Table 1
Comparison of structural features of hBChE and hAChE.

	hBChE	hAChE
Number of glycosylation sites	9/5[a] [17]	3 [54]
Presence of structure without antiparallel bundle	yes	no
Angle between helices in antiparallel bundle (average, crystal structures/MD simulations)	14°/11°	9°/9°
Number of hydrophobic interactions at dimerization interface, including π-cation and π-π interactions	5	12
ΔSASA, Å^2 (crystal structures/MD simulations)	−751/[-650;-800]	−1211/[-1150;-1300]
Number of stabilizing residues in loops (from FEP calculations)	4	9
Number of stabilizing residues in helices (from FEP calculations)	8	7
Number of macro-states of the α13-α18 loop	4	1
Free energy of oligomerization, kcal/mol (from REMD–US calculations)	−15.5	−26.4

[a] Native hBChE has 9 glycosylation sites, but the construct of hBChE used to obtain PDB ID 1P0I crystal structure is partially deglycosylated, and has only 5 glycosylation sites [17].

$$E_{AB} = E_{noB} - E_A + E_{noA} - E_B + E_{Coul} \quad (2)$$

$$E_{desolv} = E_{noB} - E_A \quad (3)$$

Where E_A is the energy of monomer A, E_B that of monomer B, E_{noA} — energy of dimer with zero charges on A monomer. E_{noB} — energy of dimer with zero charges on B monomer, E_{Coul} is the Coulomb energy of binding and E_{desolv} is desolvation energy.

It is possible to summarize Coulomb contributions for different groups of atoms and to identify the most contributing atoms and amino acid residues. To address this, we analyzed interactions in dimerization domains for all atoms of the helices and adjacent loops.

2.6. Markov chain analysis of molecular dynamics trajectories

To analyze conformational changes in protein subunits along unconstrained MD trajectories, the Markov chain approach [43] was used. In this study, Markov state models were constructed using PyEMMA software [44]. As features of the protein backbone dihedrals of residues 374–382 (BChE numeration) were selected. This is because among the segments that contribute significantly to Coulombic attraction, this loop is the most flexible. The time-lagged independent component analysis (TICA) algorithm was used to reduce dimensions [45], and the *k*-means clustering method was used to construct 100 microstates. The lag time was chosen as 1 ns. Microstates were clustered into 4 metastable macrostates by means of PCCA+ [46]. The transition pathways were computed by discrete transition path theory in its Markov state model (MSM) formulation [47]. To validate our results, the Chapman-Kolmogorov test [48] was implemented.

2.7. Replica exchange molecular dynamics

The replica exchange molecular dynamics method umbrella sampling (REMD-US) [24,25] was used to compute the free energy of hAChE and BChE oligomerization. As a collective variable, the distance between the centers of mass of monomers (COM, reaction coordinate) was chosen. To generate an initial path of dimer dissociation, a harmonic potential was applied along the reaction coordinate. Paths obtained for hAChE and BChE were divided into 124 windows for initial coordinates of the replicas. All replicas were simulated concurrently having Hamiltonians with different biasing potentials. A harmonic restrain force of 25 kcal/mol·Å^2 was applied. Every 100 steps replicas of the system underwent exchange performed using the Metropolis Monte Carlo criterion. Simulations were performed until full convergence during 15 ns for each replica. To construct PMF the weighted histogram analysis method (WHAM) [49,50] in the A. Grossfield implementation (v. 2.0.9, http://membrane.urmc.rochester.edu/content/wham) was used. Binding free energies were calculated from obtained PMFs according to [51,52].

2.8. In silico alanine screening

For residues within the dimerization interfaces, computational alanine scanning was performed by the FEP method, using the VMD *AlaScan* plugin [53] in Host-Guest mode. Side chains of selected residues were gradually transformed to –CH_3 groups with 20 intermediate λ-states, 1 ns MD run per state, Forward and backward runs were performed to ensure convergency.

3. Results and discussion

The least computationally demanding way to assess protein-protein binding is docking. Among the most popular programs and web-services are PyDock, Rosetta and ClusPro. All these programs use scoring functions, which can be used only to compare the stability of complexes built from the same monomers, not to compare the binding energies of homo-dimers of different proteins. The HADDOCK program was used to describe quantitatively energy of binding, but obtained dimerization energies for different AChEs, and between hAChE and hBChE were practically indistinguishable. Therefore, for quantitative comparison, more accurate and time-demanding calculations were implemented, which could describe the protein dynamics during oligomerization.

Before providing a detailed comparison of the dimerization of ChE monomers, and of the organization of the four-helix bundle, for AChE and BChE, we provide in Table 1 a brief summary of the published data and of our results.

3.1. Comparison of sequences

hAChE shares 88% identity with mAChE, 57% identity with *Tc*AChE, and 50% identity with hBChE. The residues involved in the interactions forming the four-helix bundle are largely conserved between different AChEs, whereas comparing BChE with AChEs, there are more differences (Table 2). In BChE there are more aromatic residues, and in the middle of the bundle there are some hydrophilic amino acids not seen in AChE. The four-helix bundles are bound together with a long “zip-lock” hydrophobic interface between each pair of 2-α-helix units and with electrostatic interactions in the adjacent loops. Thus, this difference in the BChE amino acid sequence should destabilize dimers. The most dramatic examples of these destabilizing changes in hBChE helices compared to hAChE, are replacements: Ala375Lys, Ala377Ser, Leu386Val, Ala530Arg. In addition, there are some important replacements in the adjacent loops: His387Asp, Pro388Asp, Gly523Lys.

3.2. The crossing angle between neighboring helices

If the crossing angle between principle axes of neighboring helices is less than 20°, it permits pairs of helices to form tight contacts [55]. We measured the crossing angle between neighboring helices α13 of one monomer and α18-19 of another monomer in crystal structures and

Table 2
Amino acid sequence of helices involved in the four-helix bundle in AChEs and in hBChE.

Protein	α13	loop1	loop2	α18
hAChE	D L A A E A V V L H Y	T D W L H P	R G L R	A Q A C A F W N R F L P K L L S A T
mAChE	D L A A E A V V L H Y	T D W L H P	R G L R	A Q T C A F W N R F L P K L L S A T
*Tc*AChE	D L G L D A V T L Q Y	T D W M D D	Q R L R	V Q M C V F W N Q F L P K L L N A T
hBChE	E F G K E S I L F H Y	T D W V D D	T K L R	A Q Q C R F W T S F F P K V L E

Shaded are the positions where amino acids in BChE differ from AChE amino acids by polarity and/or aromaticity. Colors correspond to the FEP calculation (see below): green — residues, stabilizing dimer (their replacement with Ala is unfavorable, ΔΔG > 0), red — destabilizing residues, their replacement with Ala increases stability (ΔΔG < 0).
Residues numbering:
hAChE: α13(372–382), loop1(383–388), loop2(522–525), α18(526–543).
mAChE: α13(372–382), loop1(383–388), loop2(522–525), α18(526–543).
*Tc*AChE: α13(365–375), loop1(376–381), loop2(514–517), α18(518–535).
hBChE: α13(363–373), loop1(374–379), loop2(512–515), α18(516–529).

Table 3
Angle between helices in bundle in crystal structures and during MD simulations.

Protein	Angle between α-helices α13 of monomer A and α18 of monomer B, crystal structures	Angle between α-helices α13 of monomer A and α18 of monomer B, MD trajectories
hAChE (PDB IDs 4EY4, 5FPQ, 4EY5, 4M0F,4M0E, 1B41)	9 ± 2°	9 ± 4° (normal distribution with p > 0.05)°
mAChE(PDB IDs 1MAA, 1KU6, 5DTI, 1J06)	6 ± 4°	9 ± 3°(normal distribution with p > 0.05)°
*Tc*AChE(PDB IDs 1W75, 6G1U, 1EA5, 2J3D, 1FSS, 1W75)	15 ± 4°	14 ± 4°
hBChE (glycosylated)(PDB IDs 4AQD, 5K5E, 4XII, 5DYT, 4TPK)	14 ± 3°	11 ± 4°

over MD trajectories (Table 3).

Results shown in Table 3 indicate that there is no difference in the angles between helices within dimers in crystal structures compared to angles obtained from MD simulations. From the Kolmogorov-Smirnov test with $p > 0.05$, the angle between helices in hAChE and mAChE corresponds to the normal distribution, whereas the angle between helices in *Tc*AChE and hBChE is not significantly differs from that of a normally distributed population.

3.3. Hydrophobic interactions in crystal structures and during molecular dynamics simulations

In AChE, there are 12 pairs of amino acids involved in hydrophobic contacts (hAChE numbering): Leu373-Ala542, Ala377-Phe535, Leu380-Ala530, Leu380-Phe535, Trp385-Ala530, Leu386-Ala526. In BChE, due to replacements of amino acids at equivalent positions by charged or polar ones, some of these pairs are abscent (Table 4).

There is significantly less surface available for solvent in the dimerization interface (ΔSASA— difference between SASA values of dimer and two monomers) in BChE, compared to AChE crystal structures. Calculation of ΔSASA values along MD trajectories follow similar patterns. ΔSASA values for crystal structures are within the range, observed in MD trajectories. This suggests that during MD simulations in water solution, the structure of the dimer interface is not significantly perturbed compared to the dimer interface in the X-ray structure. (Fig. SI1).

Table 4
Number of hydrophobic interactions in crystal structures (including π-cation and π-π) in hAChE (from 7 crystal structures), mAChE, *Tc*AChE, hBChE.

Protein (PDB ID)	Number of hydrophobic interactions	ΔSASA, Å^2
hAChE (4EY4)	12	−1211
mAChE (1J06)	12	−1243
*Tc*AChE (1W75)	12	−1261
hBChE (4AQD)	5*	−751

*2 of them are π-cation interactions.

3.4. Electrostatic energy of dimerization

The polar binding energies, calculated for fixed crystal structures of ChEs, span a wide range of values (Table SI1). Polar binding energies for different crystal structures of hAChE (Table SI2) also show significant variance.

Energy of desolvation was found to be sufficiently stable. This reflects stability of the contact region between dimers. Contribution of electrostatic attraction between dimers varied widely, leading to different values of finite polar energy of binding. Calculated polar contributions to binding energy were either negative or positive, *i.e.* their contribution could be either stabilizing or destabilizing for different conformations of the same protein.

To isolate the protein regions that affect the formation of dimers, we calculated the contributions from various regions of the monomers to the electrostatic attraction (Table SI3, Table SI4). The contribution from the α-helices forming the bundle itself differs greatly depending on the protein structure, even being weakly positive in a number of cases. However, the contribution from the loops around the formed bundle is always negative and stable enough for different structures of the same protein.

In the case of hAChE, the value of the electrostatic binding energy

depends in particular on the formation of a salt bridge between α-helices (Glu376-Lys538). This bridge, however, is not stable during MD trajectories in solution: one salt bridge is formed in 53% of snapshots, two symmetrical salt bridges in 35%. Presence of this salt bridge strongly affects the overall polar energy of dimerization for the contribution of α-helices to the electrostatic attraction, but does not affect the contribution from the loops (Table SI5, Table SI6).

For BChE conformations obtained from MD trajectories, the presence of salt bridge Asp367-Lys513 affects the electrostatic energy of dimerization induced by helices, but contribution of the loops is unstable, unlike what is seen for AChEs. Salt bridge Asp367-Lys513 is not stable during the MD trajectory (one bridge is formed in 60% of snapshots, two symmetrical bridges in 4%) and has a major effect on the contribution of helices to electrostatic binding energy.

The preliminary conclusion of this analysis is that the nature of dimer stabilization in AChEs and hBChE is different:

1) in AChEs, interaction between loops are stable, in BChE contribution of loops to the polar energy of dimerization is not. However, it is hard to identify individual amino acids that are responsible for this difference;
2) apolar interactions play a great role in the AChE dimers. The surface of intermonomer contact in BChE is less hydrophobic.

The following sections clarify the difference between dimers in both enzymes.

3.5. Free energy alanine screening of cholinesterases' dimerization interface

To elucidate the role of individual amino acids in the dimerization of ChEs, we performed alanine screening using the free energy perturbation alchemical transformation method.

Fig. 2 shows that in the case of hAChE, stabilization occurs with both hydrophobic residues of helices, and salt bridge, and electrostatic interactions between helices.

Mutations of His381 and Phe531 to alanine are advantageous. These two residues are located in close proximity to each other (Fig. 3), and their interactions appear to be stabilizing. However, this statement is not supported by FEP calculations.

The close proximity of His381 and Phe531 residues suggests that when His381 is protonated, π-cation interaction is possible between their rings. Additional MD simulations and FEP calculations were performed, with His381 protonated in one monomer, and then in both of them. In both cases, protonation of His381 did not lead to dimer stabilization. On the contrary, in both cases, mutation of these residues to alanine was seen to be even more energetically advantageous. In addition, during a 100 ns unconstrained MD simulation, His381 and Phe531 remained close, but did not form π-cation interactions: while these rings occasionally were parallel, they were too far apart to form stable interactions with each other. In the neutral dimer, where one or both His381 is/are protonated, the presence of His381 leads to leakage of water molecules into a highly hydrophobic environment. This may explain the destabilizing role of this residue.

For comparison, in *Tc*AChE, instead of His381, Gln374 is present at the same location. Thus, a destabilizing contact does not exist, and Phe523 (analog of Phe531 in hAChE) contributes to stabilization (Fig. SI2).

BChE has less stabilizing amino acids in loops compared to hAChE (Fig. 4). Amino acids unfavorable for BChE dimerization are 1) polar ones (*i.e.*, serine) instead of hydrophobic in helices; 2) not exposed to the contact interface (Leu370); 3) Asp375 and Asp378, which repel each other and destabilize the loop. His372 in BChE (analog of His381 in hAChE) forms a hydrogen bond with Gln518, and is more buried; thus, it does not have the destabilizing effect observed in hAChE.

Replacement of some of the hydrophobic residues at the dimerization interface with polar residues, in particular with serine residues,

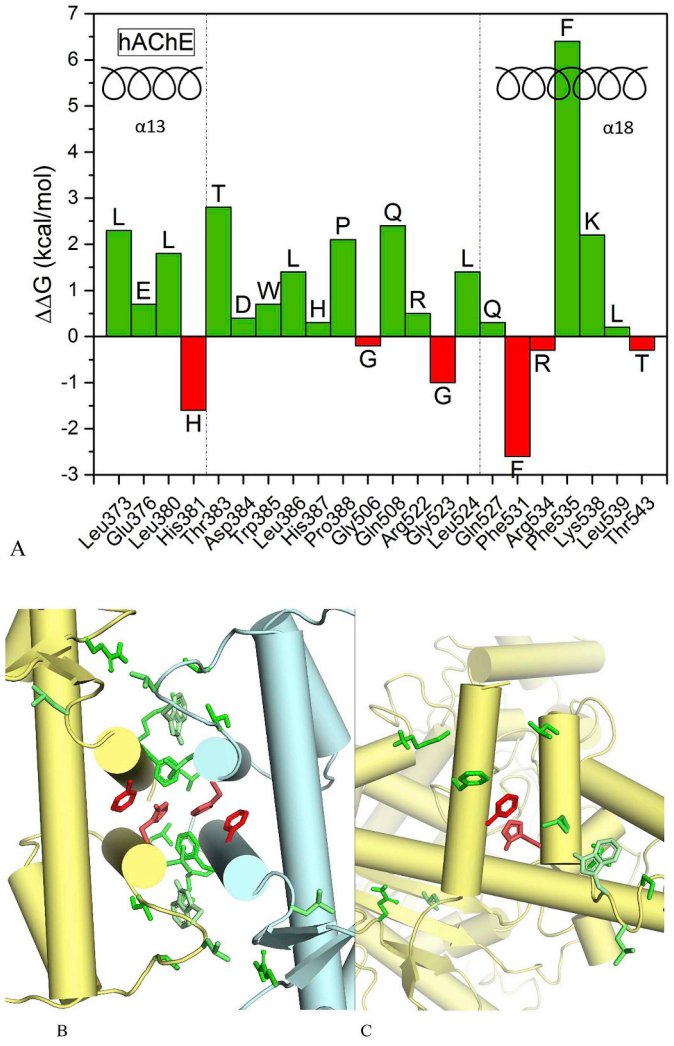

Fig. 2. *In silico* alanine screening, (FEP method), for hAChE. (A) ΔΔG values. (B) Top view of the dimerization interface of dimer; amino acids, which substitution by alanine led to $|\Delta\Delta G| > 1$ kcal/mol are shown and colored as in panel A; (C) Side view of the dimerization interface of one of the monomers, amino acids side chains are shown as in panel B.

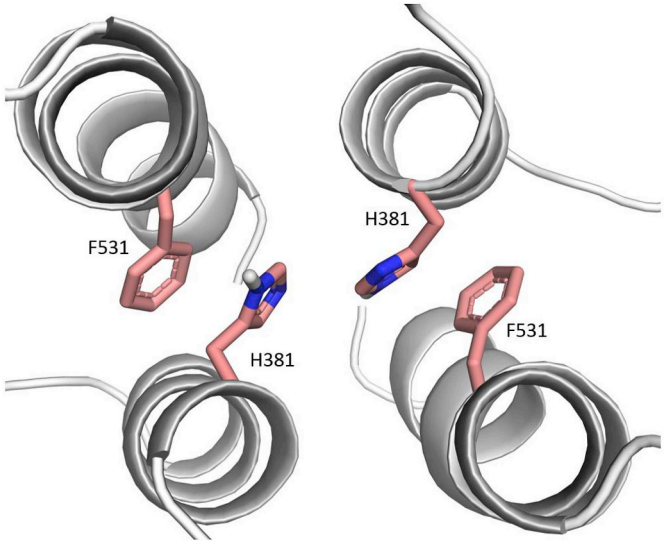

Fig. 3. Contact of His381 in the hAChE dimer, sterically stabilized by Phe531.

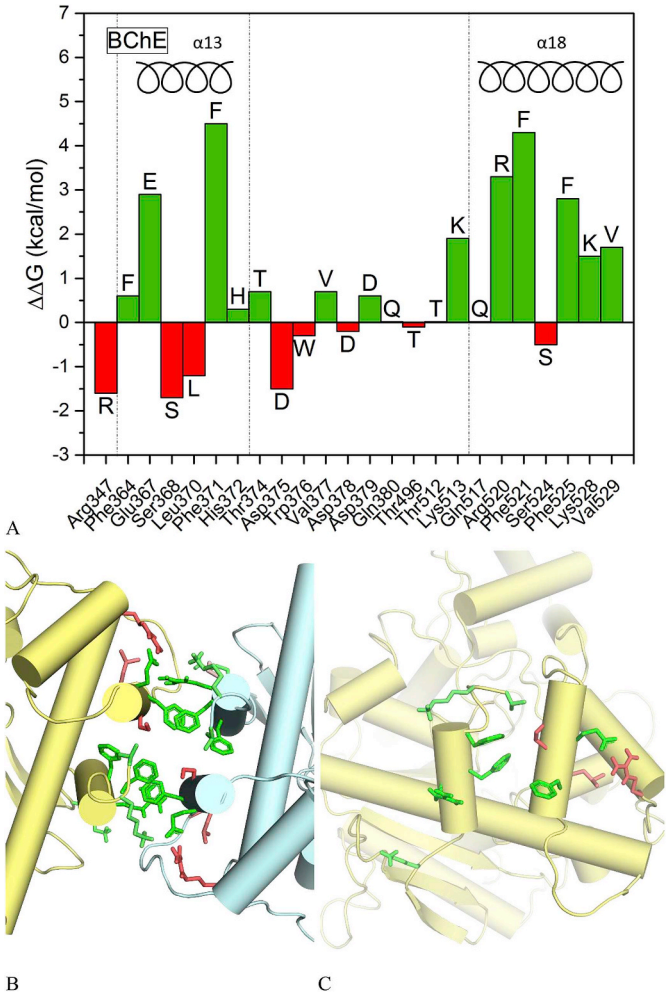

Fig. 4. *In silico* alanine screening (FEP method) for BChE. (A) ΔΔG values. (B) Top view of the dimerization interface of the dimer; the amino acids, whose substitution by alanine led to $|\Delta\Delta G| > 1$ kcal/mol are shown and colored as in panel A; (C) Side view of the dimerization interface of one monomer; the amino acids side chains are shown as in panel A.

results in inflow of water molecules into the dimerization interface. MD simulations of the BChE dimer show more water molecules in contact with hydrophobic amino acids of helices, compared to the AChE dimers. During MD simulations of the BChE dimer, water molecules constantly pass through the space between helices, reducing stability of the dimer.

Generally, *in silico* alanine screening shows that hAChE has less amino acid residues with high contribution to both stabilization and destabilization of the dimer, relative to BChE. Apart from a few residues on helices of BChE, extrahelical loops contribute to destabilization of the dimer.

3.6. Markov chain analysis of molecular dynamics trajectories

To separate the most significant contributions to the overall dimers' dynamics, we used time-lagged independent component analysis (TICA). This method allows selection of coordinates corresponding to the slowest transitions from the general MD data array, combining information from the covariance matrix and a time-lagged covariance matrix of the data. TICA analysis and following analysis of free energy landscape (computed by taking $F_i = -\ln z_i$, where z_i is the number of bin counts with corresponding values of TICAs) for hAChE and mAChE shows that there is only one macrostate (Fig. 5A). This means that the α13-α14 loop configuration is stable. For *Tc*AChE (Fig. SI3), two close macrostates were observed. There is no significant difference in forming contacts with the loop from the second monomer.

For BChE, the resulting MSM contains 100 microstates and is Markovian at 0.1 ns lag time as we saw from the plot of timescale curves. The Chapman-Kolmogorov test for 4 macrostates indicates that our model is Markovian, too. We combined 100 microstates into 4 macrostates using the PCCA + algorithm to predict the conformation dynamics of the loop (Fig. 5B). Fig. 5C and D show conformations of the loop corresponding to the four macrostates. In addition, Fig. 5E shows that the forth (yellow) conformation is closer to the second dimer than the first (red) one, so the transition between these states corresponds to transition between the more and less stabilized dimers. The red state is the stabilized state, with the hydrogen bond between Arg381 and Asp378 (which partly explains why alanine is more preferable then Asp378) and yellow is the state that is stabilized by an hydrogen bond between Trp376 and Gln380.

Dimers from the yellow cluster have an angle between α-helices from different monomers ~6.5 ± 3°, whereas dimers from the red cluster have angle between α-helices from different monomers ~14 ± 2°. This suggests that the interactions between monomers in the yellow cluster stabilize monomers in dimers in the best position for hydrophobic interactions.

In crystal structures of BChE, α13-α14 loops are not resolved with an appropriate accuracy; average B-factors of atoms in the loops differ from the average B-factors of all atoms in the protein by more than 2 SD (Table SI8).

3.7. The free energy of hAChE and BChE oligomerization by REMD-US

The free energies of dimerization of human ChEs were calculated from PMF profiles, obtained using the US-REMD protocol (Fig. 6), according to the scheme suggested in [51,52]. ΔG°_{bind} for hAChE was −26.4 kcal/mol, and far less for hBChE, −15.5 kcal/mol, reflecting reduced stability of the four-helix bundle observed in X-ray crystallography.

During dissociation of the hAChE dimer, the helices tend to be parallel. This maintains continuous hydrophobic contacts as long as possible and keeps loops close to each other. For BChE, as opposite situation is observed, *i.e.* contacts between loops are lost at the beginning of the dissociation process, while π-π and π-cation contacts in the middle of the helices are maintained.

This supports our suggestion that replacement of hydrophobic amino acids of the dimerization interface of hAChE by polar residues in BChE lowers the stability of the dimer. Thus, electrostatic interactions do not contribute significantly to dimerization. This is in agreement with early experimental observations, that the ionic strength (in the range μ = 0.001 to 1) does not affect interconversion between monomeric and disulfide-free dimeric forms of hBChE [56].

4. Conclusions

Both AChE and BChE form dimers *via* a four-helix bundle contact. For both enzymes, forces keeping monomers together include both apolar and polar contacts. Because of differences in primary and tertiary structure, the free energy of dimerization for BChE is less than that for AChE, and the contribution to the free energy of the different binding forces varies. We can distinguish two determinants for the less stable interaction contacts in BChE:

1) an unstable loop between the α 13 and α 14 helices
2) less hydrophobic surface of contact.

In crystal structures, BChE dimers with antiparallel four-helix bundle are formed less often than in hAChE. Most BChE crystal structures (76% of those in the PDB) contain dimers in which angle between the axes of the helices in the bundle are around 60°. The first dimer with

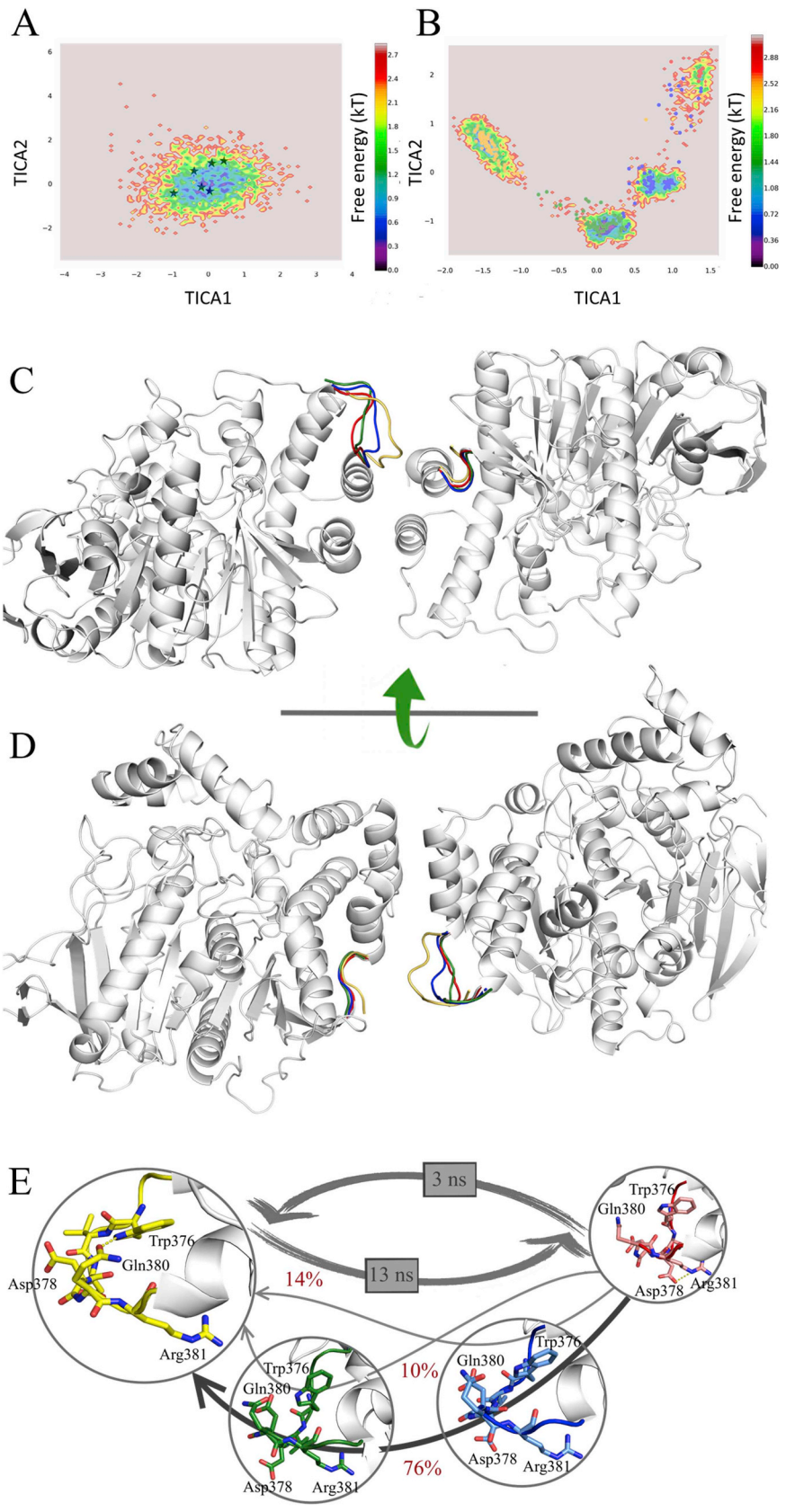

Fig. 5. (A) Free energy landscape for hAChE — only one macrostate. Stars correspond to the crystal structures (5HQ3, 4EY5, 4EY6, 4M0E, 4M0F, 5HF5), see Table SI7 for TICA 1 and TICA2 coordinates of these structures. (B) Clusters colored corresponding to macrostates on the free energy landscape for BChE. (C,D) BChE dimer, top and side view. Red loop — first macrostate, blue loop — second macrostate, green loop — third macrostate, yellow loop — forth macrostate. (E) Pathways between macrostates of the BChE 374–382 loop with the percentage of the individual paths. The gray boxes display mean first passage times. The more populated the macrostate, the larger the size of the circle.

an antiparallel four-helix bundle was obtained in 2012 [18] for fully glycosylated hBChE, with one glycan chain directly involved in stabilizing crystal structure. AChE dimers form an antiparallel type of contact without any involvement of glycan chains. This is additional evidence that the quaternary structures of AChE and BChE are very different, even though these enzymes are sisters within the cholinesterase family.

In spite of its distinctive secondary structure configuration, the four-

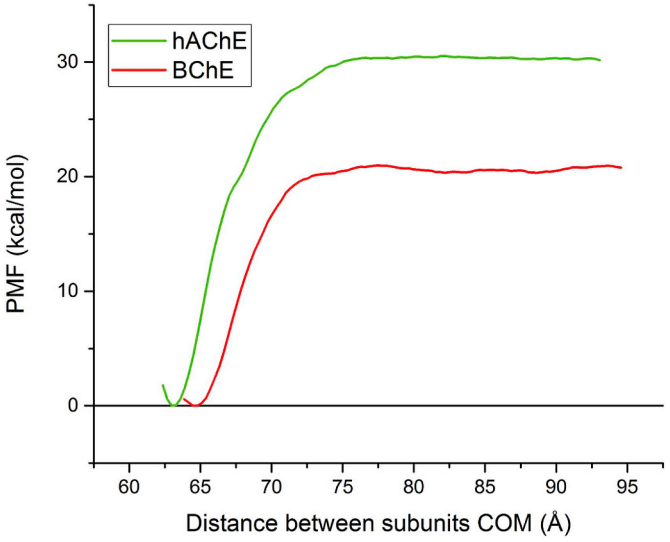

Fig. 6. PMF profile of hAChE and hBChE dimerization by REMD.

helix bundle is not a conserved motif, with an uniform type of organization of the dimerization interface; rather, the strength and nature of interactions between the monomers can be different. Stabilization of a four-helix bundle type of contact is achieved not only through interactions between the helices themselves, but also through interactions in vicinal segments; *e.g.* adjacent unstructured loops, may pay a significant role in stabilizing or destabilizing the dimer. It would not be surprising if this significant difference in the orientation of the dimers, as described in this study, between AChE and BChE played a key role in the functional difference between these two closely related enzymes, with such similar tertiary structures.

Declaration of interests

The authors declare that they have no known competing financial interests or personal relationships that could have appeared to influence the work reported in this paper.

Acknowledgements

The research was carried out using the equipment of the shared research facilities of HPC computing resources at Lomonosov Moscow State University. We acknowledge the Joint Supercomputer Center of the Russian Academy of Sciences for provision of computational time. We thank Dr. I.V. Polyakov for his help.

The reported study was funded by RFBR according to the research project №19-03-00043 to DN and SL.

Appendix A. Supplementary data

Supplementary data to this article can be found online at https://doi.org/10.1016/j.cbi.2019.06.012.

Transparency document

Transparency document related to this article can be found online at https://doi.org/10.1016/j.cbi.2019.06.012

References

[1] J. Massoulie, The origin of the molecular diversity and functional anchoring of cholinesterases, Neurosignals 11 (2002) 130–143, https://doi.org/10.1159/000065054.

[2] J. Massoulie, N. Perrier, H. Noureddine, D. Liang, S. Bon, Old and new questions about cholinesterases, Chem. Biol. Interact. 175 (2008) 30–44, https://doi.org/10.1016/j.cbi.2008.04.039.

[3] O. Lockridge, Review of human butyrylcholinesterase structure, function, genetic variants, history of use in the clinic, and potential therapeutic uses, Pharmacol. Therapeut. 148 (2015) 34–46, https://doi.org/10.1016/j.pharmthera.2014.11.011.

[4] T. Chitlaru, C. Kronman, B. Velan, A. Shafferman, Effect of human acetylcholinesterase subunit assembly on its circulatory residence, Biochem. J. 354 (2001) 613–625, https://doi.org/10.1042/bj3540613.

[5] K. MacPhee-Quigley, T.S. Vedvick, P. Taylor, S.S. Taylor, Profile of the disulfide bonds in acetylcholinesterase, J. Biol. Chem. 261 (1986) 13565–13570.

[6] W.L. Roberts, B.P. Doctor, J.D. Foster, T.L. Rosenberry, Bovine brain acetylcholinesterase primary sequence involved in intersubunit disulfide linkages, J. Biol. Chem. 266 (1991) 7481–7487.

[7] O. Lockridge, S. Adkins, B.N. Ladu, Location of disulfide bonds within the sequence of human-serum cholinesterase, J. Biol. Chem. 262 (1987) 12945–12952.

[8] H. Noureddine, S. Carvalho, C. Schmitt, J. Massoulie, S. Bon, Acetylcholinesterase associates differently with its anchoring proteins ColQ and PRiMA, J. Biol. Chem. 283 (2008) 20722–20732, https://doi.org/10.1074/jbc.M801364200.

[9] G. Gibney, P. Taylor, Biosynthesis of Torpedo acetylcholinesterase in mammalian cells. Functional expression and mutagenesis of the glycophospholipid-anchored form, J. Biol. Chem. 265 (1990) 12576–12583.

[10] P. Marchot, R.B. Ravelli, M.L. Raves, Y. Bourne, D.C. Vellom, J. Kanter, S. Camp, J.L. Sussman, P. Taylor, Soluble monomeric acetylcholinesterase from mouse: expression, purification, and crystallization in complex with fasciculin, Protein Sci. 5 (1996) 672–679, https://doi.org/10.1002/pro.5560050411.

[11] G. Kryger, M. Harel, K. Giles, L. Toker, B. Velan, A. Lazar, C. Kronman, D. Barak, N. Ariel, A. Shafferman, I. Silman, J.L. Sussman, Structures of recombinant native and E202Q mutant human acetylcholinesterase complexed with the snake-venom toxin fasciculin-II, Acta Crystallogr. D Biol. Crystallogr. 56 (2000) 1385–1394, https://doi.org/10.1107/s0907444900010659.

[12] H. Chaabihi, D. Fournier, Y. Fedon, J.P. Bossy, M. Ravallec, G. Devauchelle, M. Cerutti, Biochemical characterization of Drosophila melanogaster acetylcholinesterase expressed by recombinant baculoviruses, Biochem. Biophys. Res. Commun. 203 (1994) 734–742, https://doi.org/10.1006/bbrc.1994.2243.

[13] R.M. Blong, P. Masson, O. Lockridge, Subunit association and stabilization of butyrylcholinesterase (BChE), in: D.M. Quinn, A.S. Balasubramanian, B.P. Doctor, P. Taylor (Eds.), Enzymes of the Cholinesterase Family, Springer, Boston, MA, 1995, pp. 129–130.

[14] P. Masson, Multiple molecular forms of human plasma butyrylcholinesterase I. Apparent molecular parameters and broad pattern of the quaternary structure, Biochim. Biophys. Acta Protein Struct. 578 (1979) 493–504, https://doi.org/10.1016/0005-2795(79)90179-X.

[15] H.M. Berman, The protein data bank, Nucleic Acids Res. 28 (2000) 235–242, https://doi.org/10.1093/nar/28.1.235.

[16] Y. Nicolet, O. Lockridge, P. Masson, J.C. Fontecilla-Camps, F. Nachon, Crystal structure of human butyrylcholinesterase and of its complexes with substrate and products, J. Biol. Chem. 278 (2003) 41141–41147, https://doi.org/10.1074/jbc.M210241200.

[17] F. Nachon, Y. Nicolet, N. Viguié, P. Masson, J.C. Fontecilla-Camps, O. Lockridge, Engineering of a monomeric and low-glycosylated form of human butyrylcholinesterase, Eur. J. Biochem. 269 (2002) 630–637, https://doi.org/10.1046/j.0014-2956.2001.02692.x.

[18] X. Brazzolotto, M. Wandhammer, C. Ronco, M. Trovaslet, L. Jean, O. Lockridge, P.Y. Renard, F. Nachon, Human butyrylcholinesterase produced in insect cells: huprine-based affinity purification and crystal structure, FEBS J. 279 (2012) 2905–2916, https://doi.org/10.1111/j.1742-4658.2012.08672.x.

[19] H. Dvir, M. Harel, S. Bon, W.Q. Liu, M. Vidal, C. Garbay, J.L. Sussman, J. Massoulie, I. Silman, The synaptic acetylcholinesterase tetramer assembles around a polyproline II helix, EMBO J. 23 (2004) 4394–4405, https://doi.org/10.1038/sj.emboj.7600425.

[20] M.R. Leung, L.S. van Bezouwen, L.M. Schopfer, J.L. Sussman, I. Silman, O. Lockridge, T. Zeev-Ben-Mordehai, Cryo-EM structure of the native butyrylcholinesterase tetramer reveals a dimer of dimers stabilized by a superhelical assembly, Proc. Natl. Acad. Sci. U. S. A. 115 (2018) 13270–13275, https://doi.org/10.1073/pnas.1817009115.

[21] K.M. Boyko, T.N. Baymukhametov, Y.M. Chesnokov, M. Hons, S.V. Lushchekina, P.V. Konarev, A.V. Lipkin, A.L. Vasiliev, P. Masson, V.O. Popov, M.V. Kovalchuk, 3D structure of the natural tetrameric form of human butyrylcholinesterase as revealed by cryoEM, SAXS and MD, Biochimie 156 (2019) 196–205, https://doi.org/10.1016/j.biochi.2018.10.017.

[22] R.W. Zwanzig, High-temperature equation of state by a perturbation method. I. Nonpolar gases, J. Chem. Phys. 22 (1954) 1420–1426, https://doi.org/10.1063/1.1740409.

[23] V. Ramadoss, F. Dehez, C. Chipot, AlaScan: a graphical user interface for alanine scanning free-energy calculations, J. Chem. Inf. Model. 56 (2016) 1122–1126, https://doi.org/10.1021/acs.jcim.6b00162.

[24] B. Roux, The calculation of the potential of mean force using computer-simulations, Comput. Phys. Commun. 91 (1995) 275–282, https://doi.org/10.1016/0010-4655(95)00053-I.

[25] R. Zhou, Replica exchange molecular dynamics method for protein folding simulation, Methods Mol. Biol. 350 (2007) 205–223, https://doi.org/10.1385/1-59745-189-4:205.

[26] T. UniProt Consortium, UniProt: the universal protein knowledgebase, Nucleic Acids Res. 46 (2018) 2699, https://doi.org/10.1093/nar/gky092.

[27] J. Cheung, M.J. Rudolph, F. Burshteyn, M.S. Cassidy, E.N. Gary, J. Love, M.C. Franklin, J.J. Height, Structures of human acetylcholinesterase in complex

with pharmacologically important ligands, J. Med. Chem. 55 (2012) 10282–10286, https://doi.org/10.1021/jm300871x.
[28] Y. Bourne, P. Taylor, Z. Radic, P. Marchot, Structural insights into ligand interactions at the acetylcholinesterase peripheral anionic site, EMBO J. 22 (2003) 1–12, https://doi.org/10.1093/emboj/cdg005.
[29] H.M. Greenblatt, C. Guillou, D. Guenard, A. Argaman, S. Botti, B. Badet, C. Thal, I. Silman, J.L. Sussman, The complex of a bivalent derivative of galanthamine with torpedo acetylcholinesterase displays drastic deformation of the active-site gorge: implications for structure-based drug design, J. Am. Chem. Soc. 126 (2004) 15405–15411, https://doi.org/10.1021/ja0466154.
[30] N. Eswar, B. Webb, M.A. Marti-Renom, M.S. Madhusudhan, D. Eramian, M.Y. Shen, U. Pieper, A. Sali, Comparative protein structure modeling using Modeller (Chapter 5), Curr. Protoc. Bioinf. (2006), https://doi.org/10.1002/0471250953.bi0506s15 Unit-5 6.
[31] J.M. Word, S.C. Lovell, T.H. LaBean, H.C. Taylor, M.E. Zalis, B.K. Presley, J.S. Richardson, D.C. Richardson, Visualizing and quantifying molecular goodness-of-fit: small-probe contact dots with explicit hydrogen atoms, J. Mol. Biol. 285 (1999) 1711–1733, https://doi.org/10.1006/jmbi.1998.2400.
[32] W. Humphrey, A. Dalke, K. Schulten, VMD: visual molecular dynamics, J. Mol. Graph. 14 (1996) 33–38, https://doi.org/10.1016/0263-7855(96)00018-5.
[33] J.C. Phillips, R. Braun, W. Wang, J. Gumbart, E. Tajkhorshid, E. Villa, C. Chipot, R.D. Skeel, L. Kale, K. Schulten, Scalable molecular dynamics with NAMD, J. Comput. Chem. 26 (2005) 1781–1802, https://doi.org/10.1002/jcc.20289.
[34] R.B. Best, X. Zhu, J. Shim, P.E. Lopes, J. Mittal, M. Feig, A.D. Mackerell Jr., Optimization of the additive CHARMM all-atom protein force field targeting improved sampling of the backbone phi, psi and side-chain chi(1) and chi(2) dihedral angles, J. Chem. Theory Comput. 8 (2012) 3257–3273, https://doi.org/10.1021/ct300400x.
[35] V.V. Voevodin, S.A. Zhumatiy, S.I. Sobolev, A.S. Antonov, P.A. Bryzgalov, D.A. Nikitenko, K.S. Stefanov, V.V. Voevodin, Practice of "Lomonosov" supercomputer, Open Syst. J. 7 (2012), http://www.osp.ru/os/2012/2007/13017641/.
[36] S.J. Wodak, J. Janin, Analytical approximation to the accessible surface area of proteins, Proc. Natl. Acad. Sci. U. S. A. 77 (1980) 1736–1740, https://doi.org/10.1073/pnas.77.4.1736.
[37] E. Jurrus, D. Engel, K. Star, K. Monson, J. Brandi, L.E. Felberg, D.H. Brookes, L. Wilson, J. Chen, K. Liles, M. Chun, P. Li, D.W. Gohara, T. Dolinsky, R. Konecny, D.R. Koes, J.E. Nielsen, T. Head-Gordon, W. Geng, R. Krasny, G.W. Wei, M.J. Holst, J.A. McCammon, N.A. Baker, Improvements to the APBS biomolecular solvation software suite, Protein Sci. 27 (2018) 112–128, https://doi.org/10.1002/pro.3280.
[38] R.D. Gorham Jr., C.A. Kieslich, A. Nichols, N.U. Sausman, M. Foronda, D. Morikis, An evaluation of Poisson-Boltzmann electrostatic free energy calculations through comparison with experimental mutagenesis data, Biopolymers 95 (2011) 746–754, https://doi.org/10.1002/bip.21644.
[39] D. Sitkoff, K.A. Sharp, B. Honig, Accurate calculation of hydration free-energies using macroscopic solvent models, J. Phys. Chem. 98 (1994) 1978–1988, https://doi.org/10.1021/j100058a043.
[40] K. Lindorff-Larsen, S. Piana, K. Palmo, P. Maragakis, J.L. Klepeis, R.O. Dror, D.E. Shaw, Improved side-chain torsion potentials for the Amber ff99SB protein force field, Proteins 78 (2010) 1950–1958, https://doi.org/10.1002/prot.22711.
[41] T.J. Dolinsky, P. Czodrowski, H. Li, J.E. Nielsen, J.H. Jensen, G. Klebe, N.A. Baker, PDB2PQR: expanding and upgrading automated preparation of biomolecular structures for molecular simulations, Nucleic Acids Res. 35 (2007) W522–W525, https://doi.org/10.1093/nar/gkm276.
[42] F. Dong, H.X. Zhou, Electrostatic contribution to the binding stability of protein-protein complexes, Proteins 65 (2006) 87–102, https://doi.org/10.1002/prot.21070.
[43] G.R. Bowman, X. Huang, V.S. Pande, Network models for molecular kinetics and their initial applications to human health, Cell Res. 20 (2010) 622–630, https://doi.org/10.1038/cr.2010.57.
[44] M.K. Scherer, B. Trendelkamp-Schroer, F. Paul, G. Perez-Hernandez, M. Hoffmann, N. Plattner, C. Wehmeyer, J.H. Prinz, F. Noe, PyEMMA 2: a software package for estimation, validation, and analysis of Markov models, J. Chem. Theory Comput. 11 (2015) 5525–5542, https://doi.org/10.1021/acs.jctc.5b00743.
[45] G. Perez-Hernandez, F. Paul, T. Giorgino, G. De Fabritiis, F. Noe, Identification of slow molecular order parameters for Markov model construction, J. Chem. Phys. 139 (2013) 015102, https://doi.org/10.1063/1.4811489.
[46] S. Roblitz, M. Weber, Fuzzy spectral clustering by PCCA plus : application to Markov state models and data classification, Adv. Data Anal. Classif. 7 (2013) 147–179, https://doi.org/10.1007/s11634-013-0134-6.
[47] F. Noe, C. Schutte, E. Vanden-Eijnden, L. Reich, T.R. Weikl, Constructing the equilibrium ensemble of folding pathways from short off-equilibrium simulations, Proc. Natl. Acad. Sci. U. S. A. 106 (2009) 19011–19016, https://doi.org/10.1073/pnas.0905466106.
[48] J.H. Prinz, H. Wu, M. Sarich, B. Keller, M. Senne, M. Held, J.D. Chodera, C. Schutte, F. Noe, Markov models of molecular kinetics: generation and validation, J. Chem. Phys. 134 (2011) 174105, https://doi.org/10.1063/1.3565032.
[49] J.C. Gumbart, B. Roux, C. Chipot, Efficient determination of protein-protein standard binding free energies from first principles, J. Chem. Theory Comput. 9 (2013), https://doi.org/10.1021/ct400273t.
[50] B. Roux, The calculation of the potential of mean force using computer simulations, Comput. Phys. Commun. 91 (1995) 275–282, https://doi.org/10.1016/0010-4655(95)00053-i.
[51] J.S. Patel, F.M. Ytreberg, Fast calculation of protein-protein binding free energies using umbrella sampling with a coarse-grained model, J. Chem. Theory Comput. 14 (2018) 991–997, https://doi.org/10.1021/acs.jctc.7b00660.
[52] S. Doudou, N.A. Burton, R.H. Henchman, Standard free energy of binding from a one-dimensional potential of mean force, J. Chem. Theory Comput. 5 (2009) 909–918, https://doi.org/10.1021/ct8002354.
[53] P. Liu, F. Dehez, W. Cai, C. Chipot, A toolkit for the analysis of free-energy perturbation calculations, J. Chem. Theory Comput. 8 (2012) 2606–2616, https://doi.org/10.1021/ct300242f.
[54] B. Velan, C. Kronman, A. Ordentlich, Y. Flashner, M. Leitner, S. Cohen, A. Shafferman, N-glycosylation of human acetylcholinesterase: effects on activity, stability and biosynthesis, Biochem. J. 296 (Pt 3) (1993) 649–656, https://doi.org/10.1042/bj2960649.
[55] S. Kamtekar, M.H. Hecht, Protein Motifs. 7. The four-helix bundle: what determines a fold? FASEB J. 9 (1995) 1013–1022, https://doi.org/10.1096/fasebj.9.11.7649401.
[56] P. Masson, Formes Moléculaires Multiples et Structure Quaternaire de la Butyrylcholinestérase du Sérum Humain, Thèse de Doctorat d'Etat es-Sciences Pharmaceutiques, University Claude Bernard, Lyon, France, 1978.